Chapter 18

Characterization of Optical Fibers by Multiple-Beam Interferometry

Fouad El-Diasty

Additional information is available at the end of the chapter

http://dx.doi.org/10.5772/54720

1. Introduction

Optical fibers as circular dielectric optical waveguides made of silica glass with the lowest loss and the most carefully controlled index. Doping with impurity oxides such as Germenia GeO_2, Titania TiO_2, Caesia Cs_2O, Alumina Al_2O_3, Zirconia ZrO_2 and Phosphorus pentaoxide P_2O_5 rises the refractive index of pure silica in the core region. [1] Doping with Boria B_2O_3 or Fluorine F inferiors the refractive index of the cladding. [2] Rare-earth ions such as $ErCl_3$ and Nd_2O_3 have been used in order to make fiber amplifiers and fiber lasers. [3] Polymer optical fibers are also achieved with increased attention for short-haul transmission of light, although these fibers are limited to multi-mode dimensions. [4]- [9]

In addition to the application in fast high capacity telecommunication, optical fibers are used as sensors to measure many different quantities. [10]- [11] Fiber gratings can function as mirrors [12], in which a forward-propagating mode guided by the fiber core couples to a backward-propagating mode of the same type [13]. They also can be used as mode converters, in which one type of guided core mode couples to different type of cladding mode. [14] Great interest is being paid to fiber-optic devices like modulators, coupler and switches. [15]- [16]

1.1. Type of optical fibers

The structure (geometric shape and index profile) basically establishes the information carrying capacity of the fiber and also influences the response of the fiber to environmental perturbations. Fiber modes mean field solutions of Maxwell's equations to the transverse boundary-value problem of waves that propagate without changing shape along the fiber optical axis. In case of a single-mode fiber, the fiber sustains only one mode of propagation, whereas the total number of modes M in case of multi-mode step-index fiber is given by [17]

$$M = \frac{V^2}{2} \tag{1}$$

while in case of parabolic multi-mode GRIN fiber, the number of modes is given by:

$$M = \frac{V^2}{4} \tag{2}$$

where V is the normalized frequency which can be defined as:

$$V = \frac{2\pi\ a}{\lambda}\ (\text{N.A}) \tag{3}$$

Here a is the core radius, λ is the wavelength of propagated light and N.A is the numerical aperture which is defined as:

$$\text{N.A} = \sqrt{n_{co}^2 - n_{cl}^2} \tag{4}$$

where n_{co} and n_{cl} are the core and cladding indices, respectively. Higher number of propagated modes means higher mode dispersion and hence lower data rate and less efficient transmission. This gives the reason why the single-mode fibers are preferable in very high speed telecommunication.

The refractive index profile of graded-index (GRIN) fiber is classified by two-system parameters which are giving by

$$n(r) = n_{co}\left[1 - 2\Delta n\left(\frac{r}{a}\right)^{\alpha}\right]^{1/2} \quad \text{for } r < a \tag{5}$$

$$n(r) = n_{co}\left(1 - 2\Delta n\right)^{1/2} \quad \text{for } r > a \tag{6}$$

and

$$\Delta n = \frac{n_{co}^2 - n_{cl}^2}{2n_{co}^2} \tag{7}$$

http://dx.doi.org/10.5772/54720

or

$$\Delta n = \frac{n_{co} - n_{cl}}{n_{co}} \quad \text{for} \quad n_{co} \cong n_{cl} \text{ or } \Delta n << 1 \tag{8}$$

where r is the radial distance, and α is a parameter that describes the shape of the core index profile. Δn is a measure of the index difference between the peak refractive index at the core center $n(0)$ and the cladding refractive index. For the single-mode fiber, Δn is usually in the range of $0.2\% < \Delta n < 1.5\%$; but for multi-mode fiber, the typical range is $1\% < \Delta n < 3\%$.

1.2. Dispersion and pulse propagation in optical fibers

Since the fiber is carrying a time-varying signals that comprise of multiple frequency components, so the chromatic dispersion must be considered. A medium exhibits chromatic dispersion if the propagation constant (the logarithmic rate of change with respect to the distance in a given direction of the complex amplitude of the field component) for a wave or mode varies nonlinearly with frequency. Signal distortion caused by group-velocity dispersion occurs as the different frequency components of the signal travel with different group velocities. Thus the signal components emerg from the medium with different relative time delay. Chromatic dispersion in a single-mode of optical is caused by two dependent sources:

- Material Dispersion; the refractive indices of the materials that make up the fiber waveguide depend on the optical frequency or wavelength (i.e., $n_{co} = n_{co}(\lambda)$ and $n_{cl} = n_{cl}(\lambda)$).
- Waveguide Dispersion; the effective-index of each waveguide-mode depends on the frequency or wavelength due to frequency dependence of the mode dispersion relation (i.e., $n_{eff} = n_{eff}(\lambda)$).

Material dispersion is compensated by waveguide dispersion described by the index profile. [18]- [19]

2. Characterization of optical fibers

Characterization of optical fibers means determination of both the fiber numerical aperture and the normalized frequency. This of course requires precise and sensitive measurements of very important parameters such as the index profile of both of core and cladding, index difference Δn, and the profile shaping parameter α as in case of GRIN fiber. Many of the fiber properties such as the cutoff wavelength, connection losses, and launching efficiency are determined by the refractive index profile. Also different fiber parameters can be measured from the index profile such as the induced-birefringence in optical fibers (due to external mechanical perturbations like elongation or bending of fibers [20]- [24]) or due to irradiation of the waveguide. [25]- [32] Another fiber parameters such as acceptance angle, dispersion per unit length and modal dispersion are functions of the fiber index and they need a precise

measurement of the fiber index profiles. [17] As a result different methods and techniques for characterizing optical fibers and for determining their refractive indices have been developed.

2.1. Methods for investigation the structure and index of optical fibers

Various methods are reported and applied to characterize optical fibers. They are mainly:

1. Optical microscopy [33]- [34],
2. Scanning electron microscopy [35],
3. Transmission electron microscopy;
4. X-ray spectrometry [36],
5. Infrared spectroscopy [37],
6. Speckle interferometry [38], [39],
7. Reflection method [40],
8. Quarter wave plate method [24],
9. Two-beam interference microscopy [41],
10. Multiple-beam interference,
11. Tomographic back projection [42].
12. Laser Sheet of light and lens-fiber interferometer. [43]- [47]
13. Diffraction techniques. [48]- [50]

Among them, the most reliable and precise technique is the interferometric method. [41] From the obtained interferogram the method determines the path shift of the ray transmitted through the fiber sample (the fiber is considered as a phase object). The method resolves relatively the fiber structure in detail with a higher resolution giving more quantitative and qualitative results.

3. Interferometry

Superposition of two or more coherent waves (beams) originating from the same source, but traveling different paths, results dark and bright interference fringes. A bright fringe will be observed if the path difference between the interfering beams equals an integer number of wavelength. The beams, being in phase, reinforce each other and a constructive interference occurs. Destructive interference occurs and a dark fringe result if the interfering beams are 180° out of phase or half an integer number of wavelength. Thus, the interferograme is considered as a distribution of intensity and phase. Interferometers are classified by the number of interfering beams. There are; a) two-beam interferometers (TBI) or b) multiple-beam

http://dx.doi.org/10.5772/54720

interferometers (MBI). Semi transparent mirror or beam splitter is used to separate the beams and to produce the interfering beams.

Amplitude objects vary in their light absorption with respect to surrounding medium. They do also refraction and deviation to the light beam passing through them. In contrast, phase objects produce no variation in light intensity but differ merely from the surrounding medium by their optical thickness. Optical thickness is the multiplication of refractive index of the object n by the object's metric thickness t. Application of interferometry in the field of optical fiber research considers primarily the optical fiber waveguides as a phase object. So, the variations in the fiber refractive index or its thickness, or both do shifts in the fringe position which can be measured to get information about the fiber structure.

3.1. Two-beam interferometers

The main interferometers that were developed utilizing the two-beam interference technique are; Michelson interferometer, Twyman-Green interferometer, Mach-Zehnder interferometer, Nomarski interferometer, Pluta polarizing interference microscope, Interphako interference microscope, and Baker, Dyson, Leitz, and Zeiss-Linnik interference microscopes. [51]- [54] As in Michelson interferometer, the two interfering beams have equal amplitudes but they differ in phase (δ). The resultant intensity distribution (I) follows a cosine square law given by:

$$I = I_{\circ} \cos^2\left(\frac{\delta}{2}\right) \tag{9}$$

The fiber under study is placed in quartz cell filled with an immersion liquid of uniform and known refractive index. The fiber is introduced into the path of one of the interfering beams. If the fiber axis is chosen as the z-axis while the x-axis is perpendicular the axis fiber, the equation that describes the fringe shift due to the existence of an optical fiber inside the interferometer is given by:

$$z = \frac{2\Delta z}{\lambda}\left[\left(n_{cl} - n_L\right)\left(r_{cl}^2 - x^2\right)^{1/2} + \left(n_{co} - n_L\right)\left(r_{co}^2 - x^2\right)^{1/2}\right] \tag{10}$$

where Δz is the interfringe spacing (free spectral range between two adjacent fringes) and n_L is the refractive index of immersion liquid.

If n^{II} and $n^{\perp}$ are the mean refractive indices of the fiber for plane polarized light vibrating in two planes parallel and perpendicular to the fiber z-axis respectively, then both of n^{II} and $n^{\perp}$ and the index difference Δn, for fiber with irregular and/or non-irregular transverse sections, are given by:

$$n^{\mathrm{II}} = n_L + \frac{F^{\mathrm{II}}\lambda}{\Delta z A} \tag{11}$$

$$n^{\perp} = n_L + \frac{F^{\perp}\lambda}{\Delta z A} \tag{12}$$

and

$$\Delta n = \left(\frac{F^{\mathrm{II}} - F^{\perp}}{\Delta z} \right) \frac{\lambda}{A} \tag{13}$$

where A and F are the mean cross sectional area of the fiber and the area under the fringe shifts.

According to the interferometric slab method [55]- [64], a thin slab of thickness 0.1 - 0.5 mm is cut out perbendicular to the fiber optic axis remaining the thickness t of the slab constant over the entire slab area to within a fraction of the wavelength of light. To measure the index profile of the fiber, the slab is placed in one arm of an interference microscope, and a reference slab with a refractive index equals the cladding index is placed in the second arm of the microscope. If the two mirrors are slightly inclined, a system of equally spaced fringes with two-beam intensity distribution is formed, see Fig. 1. The core refractive index can be described by:

$$n(x,y) = n_{cl} + \frac{\lambda\lambda\ z(x,y)}{t\ \Delta z} \tag{14}$$

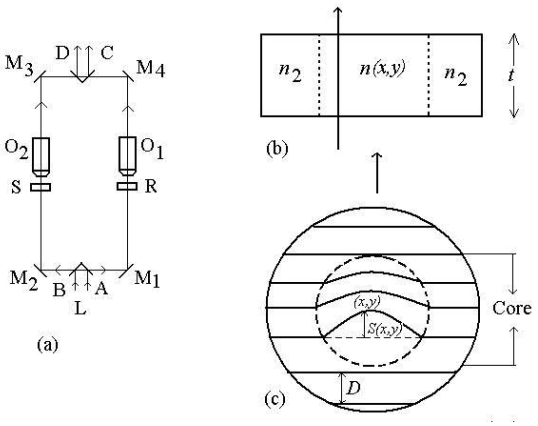

Figure 1. (a) A two-beam single-pass interference microscope. L is the incident light, M_1, M_2, M_3, and M_4 are mirrors. S is the slab, R is the reference slab, O_1 and O_2 are microscope objectives. A, B, C, and D are semi-transparent mirrors. (b) A slab of thickness t for a graded-index core with a cladding of refractive index n_2. (c) Interferogram in which the fringe shift $Z(x, y)$ in the core region is a function of point position x, y is shown.

Transverse two-beam interference technique [65]- [80] applied to study optical fibers requires the light to be incident perpendicular to the fiber axis. The fiber is immersed in a matching liquid whose refractive index is nearly equal to that of the fiber cladding. The technique avoids the time consuming for sample preparation which is needed in the slab method. The propagation problem associated with the reflection technique can be avoided.

Barakat et al. [81] used a Zeiss-Linnik as a two-beam interferometer to obtain interferograms of fusion-spliced fibers. A common feature is the presence of buckling of the fiber material on both sides of the splicing point. This resulted from the fusion splicing process. Their heights ranged from 1 to 10 μm, some 300 μm apart for graded-index fibers of 50 μm core and 125 μm cladding diameters. The power loss resulting from fusion splicing for the specimens examined interferometricaly is measured. It is found that the greater the buckling, the greater the power loss. A height of 2λ or less (λ = 535 nm) gave no detectable loss.

White-light spectral interferometric technique employing a low-resolution spectrometer is used to measure intermodal dispersion for LP_{01}^{x} and LP_{11}^{x}modes of elliptical-core optical fibers in a spectral range approximately from 540 to 870 nm. [82] The technique utilizes a tandem configuration of a Michelson interferometer and an optical fiber to measure the equalization wavelengths as a function of the optical path difference (OPD) between beams of the interferometer, or equivalently, the wavelength dependence of the intermodal group OPD in the optical fiber.

3.2. Multiple-beam interference

Multiple-beam interferometer is a device utilizes the fringes produced after multiple reflection in air film between two plates (mirrors) that thinly silvered onto their inner surfaces. The fringes (Fizeau fringes) in this case are much narrower than that in case of two-beam interference. This narrowing in the multiple-beam interference fringes gives more resolution for the spectroscopic measurements and also provides the ability to study the fine details of studied fibers and their inner structure. Fabry-Perot interferometer is an example of the multiple-beam Fizeau fringes. The two mirrors are parallel to each other to form an inner air film of constant thickness (i.e., etalon). The types of multiple-beam interference fringes that usually applied to optical fibers are:

1. multiple-beam Fizeau fringes in transmission characterized by sharp bright fringes on a dark background,
2. multiple-beam Fizeau fringes at reflection characterized by sharp dark fringes on a bright background,
3. multiple-beam fringes of equal chromatic order both in transmission and at reflection.

The theoretical expression for the intensity of the fringes was given by Airy in 1831. [83] The intensity distribution of the fringe system has the following general expression [41]

$$I = A + B + \frac{C}{1 - 2r_2 r_3 \cos\Delta + r_2 r_3} \tag{15}$$

For the transmitted system;

$$\begin{aligned} A &= B = 0 \\ C &= t_1^2 t_2^2 \end{aligned} \tag{16}$$

where A, B and C are constants depend on the used system. r_2^2 and r_3^2 are the fractions of light intensity reflected at the inner layers (glass/metal/medium and medium/metal/glass). Also t_1^2 and t_2^2 are the fractions of light intensity transmitted through the metallic layers for the upper and lower mirrors, respectively. Whereas Δ is the phase difference between any successive beams.

3.2.1. Silvered wedge interferometer

Tolansky [84] carried out analysis for the conditions needed to produce multiple-beam localized Fizeau fringes using a wedge interferometer. The successively multiple-reflected beams are not in phase in exact arithmetic series. The phase lag of the multiple-reflected beams from the arithmetic series with normal incidence is equal to [42]

$$\delta = \frac{4}{3} m^3 \varepsilon^2 \ d \tag{17}$$

where ε is the angle of the wedge, m is the order of the beam, and d is the interferometric gap thickness. To secure the Airy sum condition, the interferometric gap thickness d and the wedge angle ε must be small. The permitted limit to the phase lag (retardation) is equal to $\lambda/2$ which gives the upper limit values of d and ε. Barakat and Mokhtar [85] found out the permitted limit which gives the maximum intensity to be $\lambda/8$ which inturn brings down the upper limit of d.

3.3. Theory of transverse multiple-beam Fizeau fringes

Since the pioneer work of Barakat [86] utilizing multiple-beam Fizeau fringes to study fibers of circular cross section and composed of single and double layers, and the Fizeau interferometry has wide applications in the fiber researches. The following section is concerned with the mathematical equation of a family of Fizeau fringes across a graded-index optical fiber. The fiber is assumed to be of a perfectly circular cross section. The fiber axis is introduced in a silvered liquid wedge and the fiber is adjusted perpendicular to the apex. Both the wedge angle and the interferometric gap should be kept small to reduce the phase lag between successive beams to produce the sharpest fringes. A parallel beam of monochromatic light presented by AB and CD is incident normal to the lower mirror of the wedge. The Fiber axis

http://dx.doi.org/10.5772/54720

is chosen as the *z*-axis, and the edge of the wedge is parallel to the *x*-axis, see Fig. 2. For the optical path length (OPL) of the ray *AB* [87]

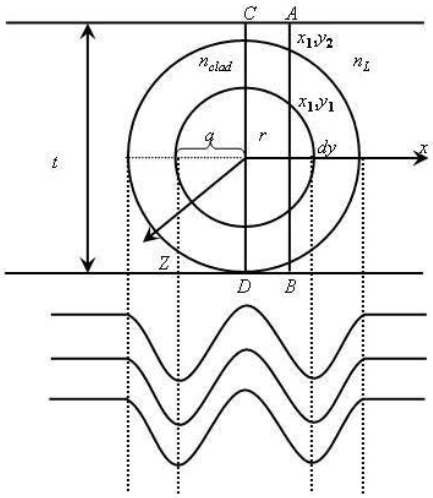

Figure 2. Cross section in a silvered liquid wedge interferometer with graded-index optical fiber of variable index core *n*(*r*). A schematic representation of the resulting fringes is shown.

$$\mathrm{OPL} = (t - 2y_2)n_L + 2(y_2 - y_1)n_{cl} + \int_0^{y_1=\sqrt{a^2-x_1^2}} n(r)\, dy, \tag{18}$$

where t is the interferometric gap thickness and $n(r)$ is the core index which is defined by Eq. (5). For index difference $\Delta n << 1$, therefore

$$\mathrm{OPL} = (t - 2y_2)n_L + 2(y_2 - y_1)n_{cl} + 2n(0)\sqrt{a^2 - x_1^2} - 2\frac{\Delta n}{a^\alpha}\int (x_1^2 + y^2)^{\alpha/2} dy \tag{19}$$

On a fringe of order of interference N,

$$N\lambda = 2(\mathrm{OPL}) = 2n_L t + 4y_2(n_{cl} - n_L) + 4\Delta n y_1 - \frac{4\Delta n}{a^\alpha}\int_0^{\sqrt{a^2-x_1^2}} (x_1^2 + y^2)^{\alpha/2} dy \tag{20}$$

For $t = z \tan \varepsilon$

$$(N\lambda \quad -2n_L z\ \tan\ \varepsilon\ ) = 4y_2(n_{cl} - n_L) + 4\Delta n y_1 - \frac{4\Delta n}{a^\alpha}\int_0^{\sqrt{a^2-x_1^2}} (x_1^2 + y^2)^{\alpha/2} dy \tag{21}$$

Transforming to the point (0, $N\lambda/2n_L$ tanε) it gives

$$z \cdot 2n_L\ \tan\varepsilon = 4y_2\left(n_{cl} - n_L\right) + 4\Delta n y_1 - \frac{4\Delta n}{a^\alpha}\int_0^{\sqrt{a^2-x_1^2}} \left(x_1^2 + y^2\right)^{\alpha/2} dy \tag{22}$$

The fringe spacing between any two consecutive fringes in the liquid region and is equal to $\lambda/2n_L$ tanε. If z is the fringe shift of the Nth order in the fiber region from its position in the liquid region, this leads to

$$\begin{aligned}\left(\frac{z}{\Delta z}\right)\cdot\lambda/2 &= 2\left[y_2\left(n_{cl} - n_L\right) + \Delta n y_1 - \frac{\Delta n}{a^\alpha}\int_0^{\sqrt{a^2-x_1^2}} \left(x_1^2 + y^2\right)^{\alpha/2} dy\right] \\ &= 2\left[\left(n_{cl} - n_L\right)\sqrt{r_f^2 - x_1^2} + \Delta n\sqrt{a^2 - x_1^2} \ - \frac{\Delta n}{a^\alpha}\int_0^{\sqrt{a^2-x_1^2}} \left(x_1^2 + y^2\right)^{\alpha/2} dy\right]\end{aligned} \tag{23}$$

This gives the required equation giving ($z/\Delta z$) for any value of x_1 where $0 \le x_1 \le a$ in terms of Δn and α. Substituting for $x_1 = 0$ gives the following expression

$$\left(\frac{z}{\Delta z}\right)\cdot\frac{\lambda}{2} = \left(n_{cl} - n_L\right)t_f + t_{co}\cdot\Delta n\frac{\alpha}{\left(\alpha+1\right)} \tag{24}$$

where $t_{co} = 2a$ and $t_f = 2y_2$.

In contrast with the case of step-index fibers when $\alpha = \infty$, the following equation can be given:

$$\left(\frac{z}{\Delta z}\right)\cdot\frac{\lambda}{2} = \left(n_{cl} - n_L\right)t_f + t_{co}\left(n_{co} - n_{cl}\right) \tag{25}$$

Fig. 3 illustrates an interferogram of Fizeau fringe in case of straight fiber immersed in a matching liquid and non-matching one. While in the second case the liquid index is less than that of fiber cladding. It could be seen that, the refractive index profile of the cladding of a straight fiber is symmetric at each point across the fiber cross section. Instead of measuring the fringe shift, the refractive index of a regular multi-layer fiber can be measured by another method developed by Hamza et al. [86] where it depends on measuring the enclosed area under the interference fringe shift F_{m} of m$^{\mathrm{th}}$ fiber layer and the mathematical expression is given by:

http://dx.doi.org/10.5772/54720

$$\frac{\lambda F_m}{4\Delta z} = \sum_{j=1}^{m} (n_j - n_{j-1}) A_{j,m} \tag{26}$$

where j is the number of layers and $A_{j,m}$ is the cross-sectional area of the fiber layers that is defined as

$$A_{j,m} = \int_{r_{m-1}}^{r_m} \sqrt{r_m^2 - x^2}\, dx \tag{27}$$

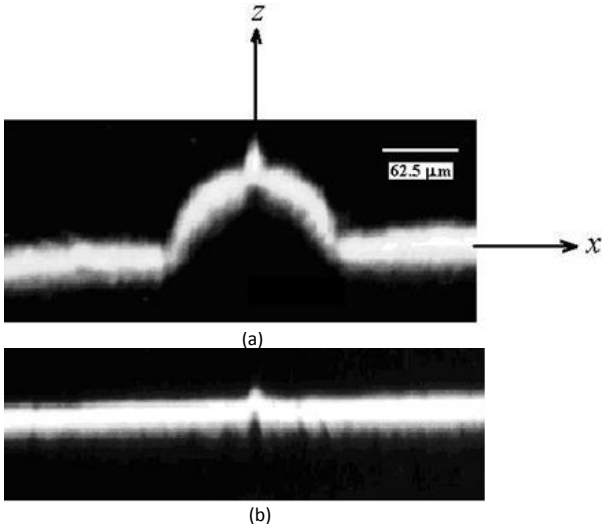

Figure 3. Interferograms of Fizeau fringe shape in case of straight fiber immersed in; (a) non-matching liquid and (b) matching liquid.

The advantage of this method is the ability to determine the refractive indices of fibers which have irregular cross-sections, where the optical properties of multiple-skin fibers of elliptical and rectangular cross sections are obtained. [88]- [91]

The minimum variance technique is used to calculate both α and Δn from the fringe shift. [92] The effect of the immersion liquid on the shape of the fringes crossing the core and the cladding has been dealt with to examine the fiber cladding and its index homogeneity, presenting a method to control the process of cladding production. [93] Barakat et al. [94] studied also the existence of successive layers forming a graded-index fiber core. Both thickness and approximate refractive index graded from one layer to another have been estimated. The fiber is found to be formed from a succession of step-index layers, $n(r)$, which remains constant over the interval thickness Δr, follows the known function relating $n(r)$ with r in terms of $n(r = 0)$ and

α, see Fig. 4. Making an analysis to the shape of a Fizeau fringe crossing GRIN fiber to its elements, it is found that the fringe is consist of two half ellipses and a saddle. [95] For a step-index fiber, the elements contributing to its fringe shape are merely two half ellipses. Using a matching liquid they could cancel the outer half ellipse in both cases. The central dip contributes an extra half ellipse and a saddle over the dip but in reverse direction away from the wedge apex. Canceling the cladding by using a matching liquid and measured the area enclosed under the core shift, an exact solution of the integration which is required to get the values of α and Δn is found. [96] An image processing system is used to analyze the multiple-beam fringes crossing optical fiber immersed in matching and non-matching liquids. [97]

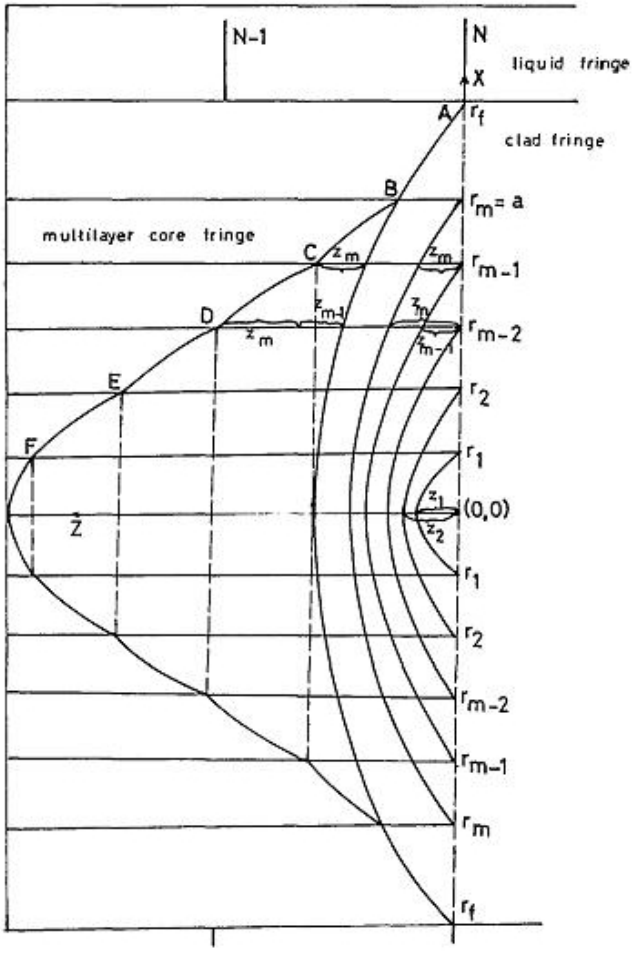

Figure 4. Shape of multi-layer core fringes, resulting from summing the contribution of each core layer in addition to the cladding of the fiber whrn immersed in a silvered liquid wedge.

http://dx.doi.org/10.5772/54720

Multiple-beam Fizeau fringes acrossing a GRIN fiber immersed in a silvered liquid wedge together with computerized optical tomographic back projection technique are used to obtain a three-dimensional refractive index profile of optical fiber core. [98] An opto-thermal device attached to automate Fizeau interferometer is used to investigate the influence of temperature on opto-thermal properties of multi-mode graded-index (GRIN) optical fiber and on fiber strucutre in a range from 27 to 54 °C. [99]- [101] Multiple-beam interferometry (MBI) of the Fizeau type is used to investigate multi-mode step-index optical fibers. Two different types of multi-mode step-index optical fibers are studied. [102]- [105] The first has a plastic cladding and silica core (the problems of studying this type of fiber and how to overcome these problems are outlined). The second fiber is a multi-mode multi-step-index (quadruple-layer) optical fiber.

Since the fringe shift across the fiber region is a function in the geometry of the different regions of the fiber and the refractive index profile of the fiber, therefore theoretical models for the fringe shift across double-clad fibers (DCFs) with rectangular, elliptical, circular, and D-shaped inner cladding are developed. [106] An algorithm to reconstruct the linear and nonlinear terms of the refractive index profile of the DCF is outlined where numerical examples are provided and discussed.

Derived mathematical expressions are used to determine the fiber dip parameters such as index difference and the dip shape parameter from interferograms of multiple-beam Fizeau fringes crossing GRIN fibers, as shown in Fig. 5. The optical fiber is of radius r_f and having a cladding of constant refractive index n_{cl}, a graded-index core of variable refractive index $n_c(r)$ and radius r_c and a graded-index dip of variable refractive index $n_d(r)$ and radius r_d. The fiber is immersed in a liquid of refractive index n_L close to n_{cl}. The equation represents the shape of multiple-beam Fizeau fringes in the dip region, i.e., for a radial distance x_1, where $0 \le x_1 \le r_d$, is given by: [107]

$$\left(\frac{z}{\Delta z}\right)_{x_1} \cdot \frac{\lambda}{2} = 2\{(n_{cl} - n_L)\sqrt{r_f^2 - x_1^2} + \Delta n_c \sqrt{r_c^2 - x_1^2} - \frac{\Delta n_c}{(r_c - r_d)^{\alpha_c}} \int_{\sqrt{r_d^2 - x_1^2}}^{\sqrt{r_c^2 - x_1^2}} \left[\sqrt{x_1^2 + y^2} - r_d\right]^{\alpha_c} dy - \Delta n_d \sqrt{r_d^2 - x_1^2} + \frac{\Delta n_d}{r_d^{\alpha_d}} \int_0^{\sqrt{r_d^2 - x_1^2}} \left(x_1^2 + y^2\right)^{\alpha_{d/2}} dy\} \quad (28)$$

where $\Delta n_c = n_c(r_d) - n_{cl}$ and α_c is a shaping parameter controlling the shape of the core index profile. Also, $\Delta n_d = n_c(r_d) - n_d(0)$and α_d is a parameter controlling the shape of the dip index profile. $\Delta z = \lambda / z n_L$ is the fringe spacing in the liquid region and z is the fringe shift in the fiber region. In the case of GRIN optical fiber having a dip of constant refractive index n_d, the

mathematical expression of the shape of Fizeau fringes across this type of optical fiber will take the form: [107]

$$\left(\frac{z}{\Delta z}\right)_{x_1} \cdot \frac{\lambda}{2} = 2\{(n_{cl} - n_L)\sqrt{r_f^2 - x_1^2} + \Delta n_c \sqrt{r_c^2 - x_1^2} - [n_c(r_d) - n_d]\sqrt{r_d^2 - x_1^2} - \frac{\Delta n_c}{(r_c - r_d)^{\alpha_c}} \int_{\sqrt{r_d^2 - x_1^2}}^{\sqrt{r_c^2 - x_1^2}} \left[\sqrt{x_1^2 + y^2} - r_d\right]^{\alpha_c} dy\} \tag{29}$$

So, in case of GRIN optical fibers having no cetral index dip Eq.(28) is converted to be Eq.(23).

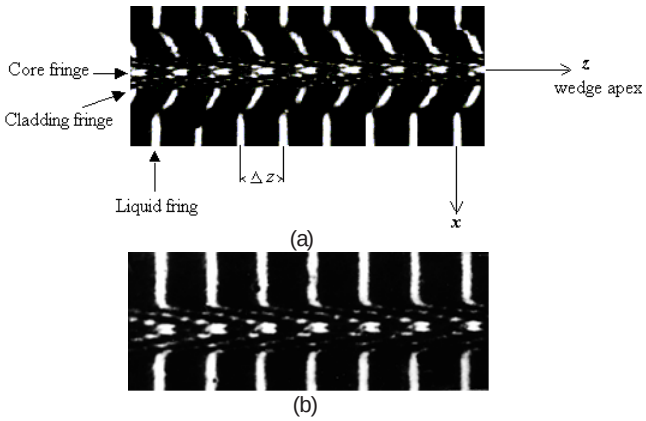

Figure 5. Multiple-beam Fizeau fringes interferogram in transmission crossing immersed GRIN fiber in a) liquid has a small refractive index than the fiber cladding and b) matched liquid.

3.4. Fiber-index determination considering refraction due to fiber layers

Fiber that being used in telecommunication has a small numerical aperture. Therefore, the change in optical path due to refraction must be taken in account to get an precise measurement of the fiber index profiles. Kahl and Mylin [108] used the ray tracing method to study analytically the effect of refractive deviation on interferograms of cylindrical and planer objects. The results indicated that the effects are additive and classified into three categories: disturbed deviation due to object only, misfocusing deviation and deviation in dense thick plates. The effect of refraction on a ray crossing the fiber perpendicular to its optic axis is studied [87]- [88] where the defocusing effect and the immersion-object index mismatch is taken into account. [109]- [111] The fringe shift and ray deflection function has been correlated to determine precisely the index profiles of preforms and optical fibers.

http://dx.doi.org/10.5772/54720

3.5. Multiple-beam interferometry for studing bent fibers

The induced-birefringence due to bending in the cladding of single-mode optical fiber has been investigated applying interferometric method. [112]- [128] Using wedge interferometer, the refractive indices for plane polarized light vibrating parallel ($\parallel$) and perpendicular ($\perp$) to the optic axis of a bent fiber represent the parameters that characterize the induced-birefringence (β) where the induced-birefringence is is given by:

$$\beta = n^{\parallel} - n^{\perp} \tag{30}$$

Considering the photo-elastic theory, the induced-birefringence as a measure of index isotropy is a second-rank tensor. It represents the changes of coefficients in the optical indicatrix or ellipsoid in the presence of applied stresses. The principal birefringence axes in case of elastic deformation coincide with the principal stress-strain axes. Fresnel's refractive index, cauchy's stress and the indicatrix or the strain ellipsoide are coaxial. [112] Due to the existence of a compression stress on one side of the fiber and a tensile stress on the other side, the fringe shift of the Fizeau fringe system of a bent single-mode optical fiber appears as anti-parallel hook-like shape fringe shifts one in each cladding side as shown schematically in Fig. 6. [113] The fringe shift $z(x)$ is considered positive in the direction of increasing n (towards the apex), while the shift is considered negative in the direction of decreasing n (away from the apex).

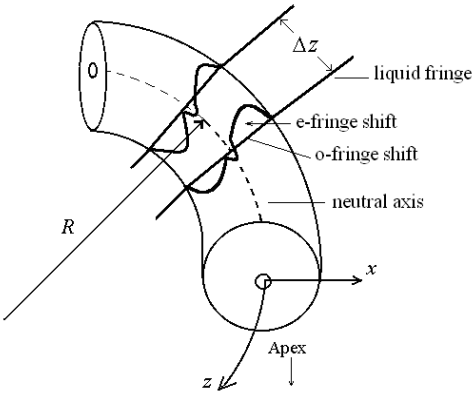

Figure 6. Schematic representation of multiple-beam Fizeau fringes in transmission applied to determine the refractive index profiles of a bent step-index optical fiber.

With a matching immersion liquid, the interferogram of the induced-birefringence of the cladding is composed of two components. One of the two fringe components ($n^{\perp}$) that represents ordinary index component shows no fringe deviation with respect to the liquid fringe position. It means that variation of the bending radius has no detectable influence on this component. Therefore $n^{\perp}$ is equal to n_L, while the shifted component (n^{II}) of β which represents the extra-ordinary index component is dependent on the radius of curvature, R.

Considering the parallel component of the refractive index of the cladding, at the compressed side of the fiber the cladding index increases and it is given by:

$$n_{cl}^{\mathrm{II}} = n_L + \frac{z_{com}(x)\lambda}{4\Delta z}\left(r^2 - x^2\right)^{-1/2} \tag{31}$$

Whereas in the tensile side of the fiber the cladding index decreases and it is described by:

$$n_{cl}^{\mathrm{II}} = n_L - \frac{z_{ten}(x)\lambda}{4\Delta z}\left(r^2 - x^2\right)^{-1/2} \tag{32}$$

The extra-ordinary component of the refractive index of bent fiber n^{II} as a function of radius of curvature is given by: [114]

$$n^{\mathrm{II}} = n_o + (n_o^3/2)[\rho_{12}(1-\nu) - \nu\rho_{11}](x/R) \tag{33}$$

where n_o is the index of straight and strain-free fiber, v is Poisson's ratio. $\rho_{11}$and ρ_{12} are the strain-optic coefficients. For a fused silica fiber ρ_{11}= 0.12, ρ_{12}= 0.27 and ν = 0.17 ± 0.02. [112], [115], [116]

The radial change of the refractive index and the related induced-birefringence in the cladding of a bent single-mode optical fiber has been measured to an accuracy of 1×10^{-4}. [113] The principal stresses in the cladding of single-mode optical fiber due to bending are demonstrated. [117] The study represented a nonlinear relation between the difference of maximum radial values of the cladding's refractive indices versus the radii of curvature in the cladding of the bent optical fibers.

The relation discribes the asymmetric distribution of the compression and tensile stresses over the fiber cross section rather than the shift in the centroid (neutral axis). An inverted *Z*-like shape has been detected in the fiber cladding between the maximum birefringence across the fiber and the radii of curvature, as shown in Fig. 7. [119] The angle between the direction of the fringe shift representing the birefringence and the radial direction provides a direct measure of the induced-birefringence. The method requires no precise polarizing optics, or complicated mechanical equipment, or variation of angle of incidence, or precise light intensity comparisons. Applying the forward scattering technique confirmed that the asymmetry distribution of the modulus value due to asymmetric index profile could be attributed to a shift in the fiber centroid (neutral axis) rather than a deviation in the circular fiber cross section due to a deformed elliptical cross section which could result under the effect of bending. Multiple-beam Fizeau interferometry is used to evaluate the acceptance angle, numerical aperture, and *V* number profiles of the bent multimode graded-index (GRIN) fiber, as shown in Fig. 8. [122]

http://dx.doi.org/10.5772/54720

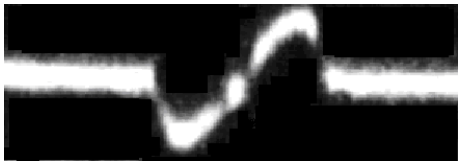

Figure 7. Interferogram of extraordinary Z-like shap fringe shift of bent sigle-mode optical fiber.

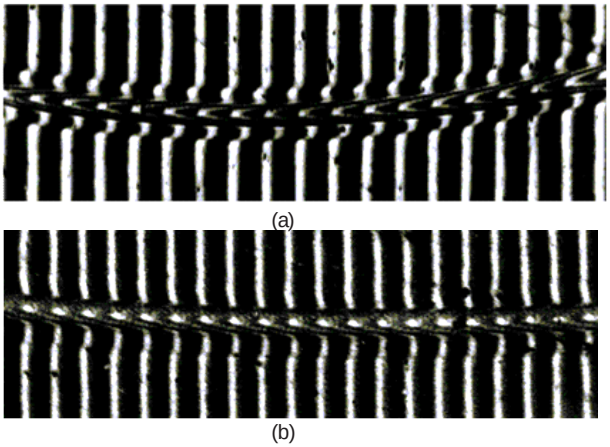

Figure 8. Multiple-beam Fizeau fringes interferogram in transmission crossing an immersed GRIN bent fiber in a) extrordinary fringe shift component and b) ordinary one.

3.6. Nonlinearity in bent optical fibers

In addition multiple-beam interferometry provides determination of nonlinearity (due to Kerr effect) in fibers such as third-order susceptibility $\chi^{(3)}$ and second-order refractive index n_2 are usually associated with all-optical effects such as modulation, soliton, switching, etc. Therefore the profiles of the induced variations of second-order refractive index and complex nonlinear third-order susceptibility components, i.e., the dispersive and absorptive are investigated in both the core and cladding of straight double-clad and macro-bent single-mode optical fibers are studied applying Fizeau interferometry. [129]- [131] The study is done on a standard single-mode fiber at two IR fundamental operating wavelengths, 1300 and 1550 nm and at radii of curvature from 5 mm to 11mm. The studies revealed an asymmetry in optical nonlinearity subsisted between the tensile and compressed sides of bent fibers due to the asymmetry in Young's modulus of the fiber material.

Multiple-beam white light interference fringes or fringes of equal chromatic orders (FECOs) are powerful and sensitive method in many field of applications. [132] The fringes are used to determine optical properties of a monomode fiber and a GRIN optical waveguide. [133]- [136]

By this method, a single interferogram of FECOs is enough to give all the needed information revealing the optical fiber parameters across the visible spectrum with sufficient accuracy.

4. Experimental setup for multiple-beam Fizeau fringes

Figs. 9 and 10 represent the wedge interferometer and setup used to produce multiple-beam Fizeau fringes in transmission. S is a low pressure Hg lamp with a green filter, L_1 is a condensing lens with a wide aperture and a short focal length, and P is an adjustable pinhole. L_2 is a collimating lens with a long focal length, W is the liquid wedge interferometer, and M is a microscope with a CCD camera attached with a PC computer. This processing enable the locateation of the peak of the fringe with an accuracy of approximately 1 pixel, i.e., 1.39 μm. The wedge interferometer consists of two circular optical flats usually 60 - 100 mm in diameter, 10 mm thick and flat to ± 0.01 μm. The inner surface of each flat is coated with a highly reflecting partially transmitting silver layer (reflectivity ≈ 70%). The two optical flats are fixed in a special jig. A drop of immersion liquid with a refractive index near by the cladding index is introduced on the sliver layer of the lower optical flat. The fiber under investigation is immersed in the liquid and the second flat is brought to form a silvered liquid wedge.

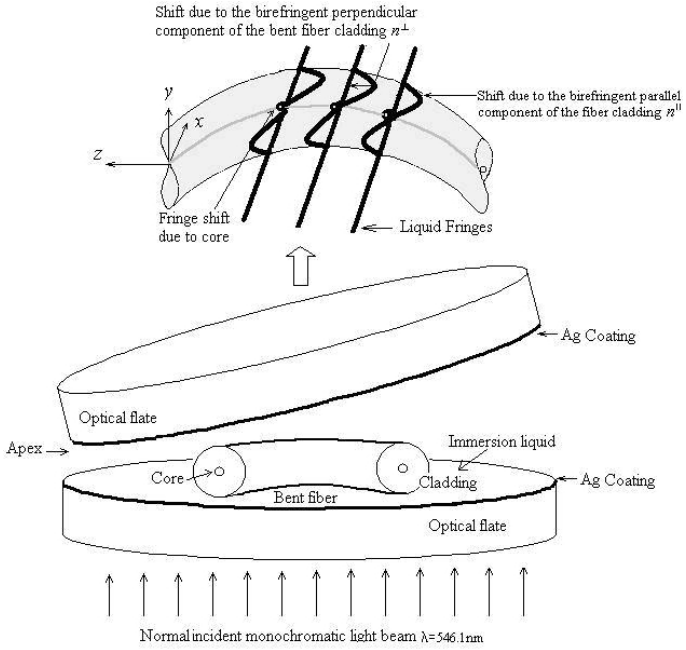

Figure 9. A schematic diagram represents the wedge interferometer and the Fizeau fringes at transmission crossing perpendicularly a bent single-mode fiber.

http://dx.doi.org/10.5772/54720

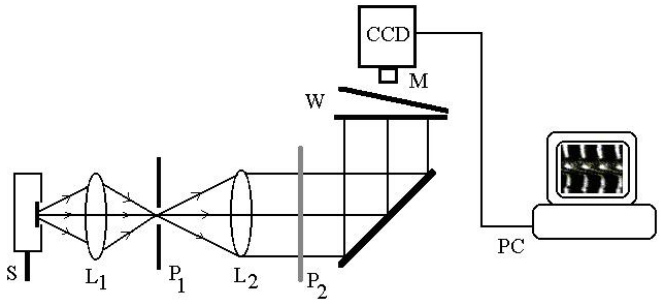

Figure 10. The optical setup for measuring the refractive index profiles of optical fibers using wedge interferometer.

A suitable immersion liquid could be prepared by mixing two different volumes of stable, clear and non-volatile liquids. α-boromonaphtalene (n = 1.6585 at 293 K) and liquid paraffine (n = 1.4500 at 293 K) might be chosen. In case of mixture of two liquids 1 and 2, the refractive index of the mixture of the immersion liquid is

$$n_L = \frac{(n_1 \mathrm{v}_1 + n_2 \mathrm{v}_2)}{\mathrm{v}_1 + \mathrm{v}_2} \tag{34}$$

where n_1 and n_2 are the refractive indices of the components, respectively. v_1 and v_2 are the volumes of the components, respectively. The interferometer is set on the microscope stage. A parallel beam of monochromatic light of known wavelength illuminates the wedge interferometer. The interferometer is adjusted so that the Fizeau fringes crossed the fiber nearly perpendicular to its optic axis, while in the liquid region they are straight lines parallel to the edge of the wedge (apex).

To obtain the sharpest fringes across the fiber, capable of revealing the fiber structure and to measure its index profile, the phase lag has to be suppressed. Both the gap thickness and the wedge angle are adjusted to reduce the phase lag and thus produce sharpest fringes across the fiber. [85]The wedge angle has to be in the range of 5×10^{-3} to 1×10^{-4} rad to be able to suppress the phase lag. The refractive index profile of the bend fiber is divide into two components; normal and parallel one. For the ordinary component (the normal one), the refractive index profile is kept unchanged similar to the case of straight fiber. But for the extra ordinary component, parallel component, the refractive index profile change across the fiber radius. In the compressed region the refractive index increases as it goes away from the fiber optic axis, i.e., neutral axis. While in tensile region, the refractive index decreases reaching its minimum values at the fiber outer surface. Fig. 11 shows interferograms of multiple-beam Fizeau fringes of the birefringence shift components in the cladding of a bent single-mode fiber immersed in a matching liquid with radius of curvature R = 9 mm. (a) the two components, (b) the perpendicular component and (c) the parallel component.

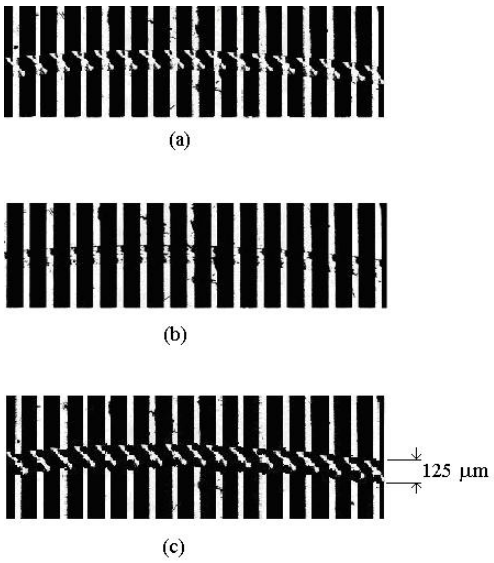

Figure 11. Interferograms of multiple-beam Fizeau fringes showing the birefringence shift components in the cladding of a bent single-mode fiber immersed in a matching liquid, R = 9 mm. (a) the two components, (b) the perpendicular component and (c) the parallel component.

5. Automatic analysis of micro-interferograms

Three different methods were usually used to analyze the fringe patterns (interferograms); traveling microscope, slide projection and image processing system. El-Zaiat and El-Hennawi [137] discussed the relative error in measuring refractive index by these methods. At constant wedge angle the relative error was ranging from 0.002 to 0.0006. Application of digital electronic provides picture acquisition, digitization and storage of the images. It also provides picture analysis, recording, printing, and reporting. Wonsiewiez et al. [63] developed a machine-aid technique of data reduction for interference micrographs. The technique was applied with the slab method and it consists of digitizing the interferogram with a scanning microdensitometer attached with computer to determine the position of the center line of each fringe. Presby et al. [64] used an automated setup of a video camera, a digitizer and computer to process the output of the interference microscope using the interferometric slab method. Many investigators used the transverse interferometric method with an immersion liquid matching to the cladding refractive index to study optical fibers electronically. [72], [73], [127], [132]- [141] A Leitz dual-beam, single-pass, transmission interference microscope is used with a video camera and video analysis system. Their measurement procedure involves video detection and digitization of interference fringes controlled by computer. The data obtained are then converted into refractive index and fiber radius information.

http://dx.doi.org/10.5772/54720

6. Conclusion

Using a silvered liquid wedge interferometer, multiple-beam Fizeau fringes at transmission crossing the fiber perpendicular to its axis suffer a shift. The shape, magnitude, and direction of the fringe shift provide quantitative and qualitative information about optical fiber structure and their index parameters. The state of polarization of the used light has an effect in the fringe shift specially in case of irregular fibers which suffer from external perturbation effects. Since the information is encoded in the phase of a fringe pattern, many practical disadvantages such as nonuniform intensity of illumination, inhomogeneous reflectivity distribution, nonlinearity of recording device, low or nonuniform contrast, and unavoidable noise affect the accuracy of determination of spatial localization of the fringe. Thus, the problem of ultra-high precise phase extraction (skeleton) is quite challenging. But the research in the field of digital fringe pattern analysis [142]- [152] is the only way to overcome this problem extending in the same time the limits of applicability of interferometry in the field of fiber researches and related devices.

Author details

Fouad El-Diasty

Department of Physics, Faculty of Science, Ain Shams University, Abbasia, Cairo, Egypt

References

[1] Midwinter, J. E. Optical fibers for transmission", (John Wiley (1979).

[2] Payne, D. N, & Gampgling, W. A. Electron. Lett. 10, 289 ((1974).

[3] Hall, D. R, & Jackson, P. E. The Physics and Technology of Laser Resonators", 1st ed. (Institute of physics publishing, Bristol and Philadelphia (1992).

[4] Ishigure, T, Nihei, E, & Koike, Y. Appl. Opt. 33, 4261 ((1994).

[5] Koike, Y, Ishigure, T, Nihei, E, & Lightwave, J. Technol. 13, 1475, ((1995).

[6] Koike, Y. nd European Conference on Optical Communication", ECOC'96, Oslo, , 1.

[7] Koike, Y, Ishigure, T, Satoh, M, & Nihei, E. th Optical Fiber Measurement Conference", OFMC'97 Teddington, UK, , 99.

[8] Koeppen, C, Shi, R. F, Chen, W. D, Garito, A. F, & Opt, J. Soc. Am. B 15, 727 ((1998).

[9] Koike, Y, Ishigure, T, Satoh, M, & Nihei, E. (1998). IEEE/LEOS Summer Topical Meeting" Monterey, CA, , 13.

[10] Decusatis, C. Opt. Eng. 37, 3082 ((1998).

[11] Dde, E. Fiber Optic Sensors: An Introduction for Scientists and Engineers", 1st ed. (Wiley, New York (1991).

[12] Erdogan, T, & Lightwave, J. Technol. 15, 1277 ((1997).

[13] Melz, G, Morey, W, & Glenn, W. H. Opt. Lett.14, 823 ((1997).

[14] Hill, K. O, Malo, B, Vineberg, K. A, Bilodeau, F, Johnson, D. C, & Skinner, I. Electron. Lett. 26, 1270 ((1990).

[15] De Paula, R. P, & Moore, E. L. In Proc. SPIE Int. Soc. Opt. Eng. 478 ((1984).

[16] Sharif, M. A. IEEE trans. Instrum. Measur. 38, 595, ((1989).

[17] Zanger, H, & Zanger, C. Fiber Optics Communication and other Applications", (Maxwell Macmillan International Publishing Group, New York, (1991).

[18] Jurgensen, K. Appl. Opt. 18, 1259 ((1979).

[19] Chang, C. T. Appl. Opt. 18, 2516 ((1979).

[20] Nagano, K, Kawakami, S, & Nishida, S. Appl. Opt. 17, 2080 ((1978).

[21] Taylor, F. F, Lightwave, J, & Technol, L. T. (1984).

[22] Sakai, J, Kimura, T, & Ieee, J. Quantum Electron. QE-17, 1041 ((1981).

[23] Smith, A. M. Appl. Opt. 19, 2606 ((1980).

[24] Ulrich, R, Rashleigh, S. C, & Eichoff, W. Opt. Lett. 5, 273 ((1980).

[25] Friebele, E. J. Opt. Eng. 18, 552 ((1979).

[26] Sigel, G. H, & Proc, J. R. IEEE 68, 1236 ((1980).

[27] Rao, R, & Mitra, S. S. Appl. Phys. Lett. 36, 948 ((1980).

[28] Friebele, E. J, Askins, C. G, & Gingerich, M. E. Appl. Opt. 23, 4202 ((1984).

[29] Chigusa, Y, Watanabe, M, Kyoto, M, Ooe, M, & Matsubara, T. IEEE Trans. Nuclear Science 35, 894 ((1988).

[30] Iida, T, Ire, S, & Sumita, K. IEEE Trans. Nuclear Science 35, 898 ((1988).

[31] Leskovar, B. IEEE Trans. Nuclear Science 36, 543 ((1989).

[32] Kyoto, M, Chigusa, Y, Ohe, M, Okamoto, S, & Lightwave, J. Technol. 10, 289 ((1992).

[33] Stoves, J. L. Fibre Microscopy", (London: National Trade Press, (1957).

[34] Francon, M. Progress in Microscopy", (Oxford: Pengamon Press, (1961).

[35] Wells, O. C. Scanning Electron Microscopy", (McGraw-Hill, New York, (1974).

[36] Kita, H, Kitano, I, Uchida, T, Furukawa, M, & Am, J. Ceramic Soc., (1971). , 54

[37] Meredith, R, & Hearle, J. W. S. Physical Methods of Investigating Textiles", (Interscience Publishers, New York, (1959).

[38] Verrier, I, & Goure, J. P. Opt. Lett. 15, 15 ((1990).

[39] Anderson, D. Z. Opt. Lett. 21, 685 ((1996).

[40] Ikeda, M, Tateda, M, & Yoshikiyo, H. Appl. Opt. 14, 814 ((1975).

[41] Barakat, N, & Hamza, A. A. Interferometry of Fibrous Materials", (Adam Hilger, Bristol and New York, (1990).

[42] Fariz, G. W, & Byer, R. L. Opt. Lett. 11, 413 ((1986).

[43] El Ghandoor, H, & Nasser, I. Afaf Abdel-Hady, A. Al-Shukri, Opti. Lasers Eng. 41, 277 ((2004).

[44] Hamza, A. A, Mabrouk, M. A, Ramadan, W. A, & Wahba, H. H. Opt. Lasers Eng. 42, 121 ((2004).

[45] Ghandoor, H, Nasserb, I, Abd-el, M. A, & Rahman, R. Hassan, Opt. Laser Technol. 32, 281 ((2000).

[46] Ghandoor, H, Abd, E, & Ghafar, R. Hassan, Opt. Laser Technol. 31, 481 ((1999).

[47] Ghandoor, H, Hennawi, H, Diasty, F, Soliman, M. A, & Mater, J. Sci. Eng. B 1, 148 ((2011).

[48] Diasty, F, & Lightwave, J. Technol. 22, 1539 ((2004).

[49] Diasty, F, Heaney, A, & Erdogan, T. Appl. Opt. 40, 890 ((2001).

[50] Thyagarajan, K. Mini Das, M. N. Satyanarayan, Opt. Commun. 218, 67 ((2003).

[51] Tolansky, S. An Introduction to Interferometry", (Longman Press, London (1973).

[52] Barakat, N, & Sorour, D. Proc. The mathematical and Physical Society of U.A.R. 28, 93 ((1966).

[53] Pluta, M. Optica Acta 18, 661 ((1971).

[54] Pluta, M, & Microsc, J. (1972).

[55] Rawson, E. G, Murray, R. G, & Ieee, J. Quantum electron. QE-9, 1114 ((1973).

[56] Martin, W. E. Appl. Opt. 13, 2112 ((1974).

[57] Cherin, A. H, Cohen, L. Q, Holden, W. S, Burrus, C. A, & Kaiser, P. Appl. Opt. 13, 2359 ((1974).

[58] Presby, H. M, & Brown, W. L. Appl. Phys. Lett. 24, 511 ((1974).

[59] Burrus, C. A, & Standley, R. D. Appl. Opt. 13, 2365 ((1974).

[60] Burrus, C. A, Chinnock, E. L, Gloge, D, Holden, W. S, Li, T, Standley, R. D, & Keck, D. B. Proc. IEEE 61, 1498 ((1973).

[61] Stone, J, & Burrus, C. A. Appl. Opt. 14, 151 ((1975).

[62] Presby, H. M, & Kaminow, I. P. Rev. Sci. Instrum. 47, 348 ((1976).

[63] Wonsiewiez, B. C, French, W. G, Lazay, P. D, & Simpson, J. R. Appl. Opt. 15, 1048 ((1976).

[64] Presby, H. M, Marcuse, D, & Astle, H. Appl. Opt. 14, 2209 ((1978).

[65] Shiraishi, S, Tanaka, G, Suzuki, S, & Kurosaki, S. Natl. Conv. Rec., IECE Japan paper 891, 239 ((1975). , 2

[66] Stone, J, & Earl, H. E. Appl. Sci. Inst. 4, 348 ((1976).

[67] Marhic, M. E, Ho, P. S, & Epstein, M. Appl. Phys. Lett. 26, 574 ((1975).

[68] Saunders, M. J, & Gardner, W. B. Appl. Opt. 16, 2369 ((1977).

[69] Iga, K, & Kokubun, Y. Tech. Digest Int. Conf., IOOC Tokyo, 403 ((1977).

[70] Kokubun, Y, & Iga, K. Trans. IEEC Japan E60, 702 ((1977).

[71] Iga, K, Kokubun, Y, & Yamamoto, N. Record of Natl. Symp. Light Radio Waves, IECE Japan paper s3-1 ((1976).

[72] Boggs, L, Presby, H. M, & Marcuse, D. Bell Syst. Tech. J. 58, 867 ((1979).

[73] Presby, H. M, Marcuse, D, Boggs, L, & Astle, H. Bell Syst. Tech. J. 58, 883 ((1979).

[74] Presby, H. M, & Opt, J. Soc. Am. 64, 280 ((1974).

[75] Presby, H. M, & Marcuse, D. Appl. Opt. 13, 2882 ((1974).

[76] Hannes, H. Koloid Z-Z Polymere 250, 765 ((1972).

[77] Witkins, L. S. Appl. Opt. 18, 2214 ((1979).

[78] Rogus, D. SPIE 1121, 317 ((1989).

[79] Bozyk, M. SPIE 1121, 284 ((1989).

[80] Pluta, M. Optica Applicata 16. 375 ((1985).

[81] Barakat, N, Hennawi, H. A, Medhat, M, Sobie, M. A, & Diasty, F. Appl. Opt. 25, 3466 ((1986).

[82] Hlubina, P. Opt. Commun. 218, 283 ((2003).

[83] Tolansky, S. Multiple-Beam Interference Microscopy of Metals", (Academic Press, London, (1970).

[84] Tolansky, S. Multiple-Beam Interferometry of Surfaces and Films (Oxford: Clarendon (1948).

[85] Barakat, N, Mokhtar, S, & Opt, J. Soc. Am. 53, 1153 ((1963).

[86] Barakat, N. Textile Res. 41, 167 ((1971).

[87] Barakat, N, Hamza, A. A, & Goneid, A. S. Appl. Opt. 24, 4383 ((1985).

[88] Hamza, A. A, Kabeel, M. A, Phys, J, & Appl, D. Phys. 19, 1175, ((1986).

[89] Hamza, A. A, Kabeel, M. A, Phys, J, & Appl, D. Phys. 20, 963, ((1987).

[90] Hamza, A. A, Sokkar, T. Z, Shahin, M. M, & Appl, J. Phys. 70, 4480 ((1991).

[91] Hamza, A. A, Mabrouk, M. A, & Modern, J. Opt. 38, 97 ((1991).

[92] Hennawi, H. A, Medhat, M, Diasty, F, & Egypt, J. Phys. 18, 179 ((1987).

[93] Hennawi, H. A, Diasty, F, Meshrif, O, & Appl, J. Phys. 62, 4931 ((1987).

[94] Barakat, N, Hennawi, H. A, & Diasty, F. Appl. Opt. 27, 5090 ((1988).

[95] Barakat, N, Hennawi, H. A, & Sobeah, H. E. Pure Appl. Opt. 2, 419, ((1993).

[96] Mabrouk, M. A, & Bawab, H. F. Pure Appl. Opt. 6, 247 ((1997).

[97] Barakat, N, Hennawi, H. A, Zaiat, S. Y, & Hassan, R. Pure Appl. Opt. 5, 27 ((1996).

[98] Barakat, N, Hennawi, H. A, Abd, E, Ghafar, H, Ghandoor, R, & Hassan, F. El-Diasty, Opt. Commun. 191, 39 ((2001).

[99] Hamza, A. A, Belal, A. E, Sokkar, T. Z. N, & Agour, H. M. E. L-D. e. s. s. o. u. k. y, M. A. Optics and Lasers Eng. 45, 145 ((2007).

[100] Hamza, A. A, Sokkar, T. Z. N, & Opt, K. A. E. L-F. a. r. a. h. a. t. y, H. M. E. L-D. e. s. s. o. u. k. y. Lasers Eng. 41, 261 ((2004).

[101] Hamza, A. A, Mabrouk, M. A, Ramadan, W. A, & Shams-eldin, M. A. Opt. Commun. 200, 131 ((2001).

[102] Hamza, A. A, & Nasr, A. M. Pure Appl. Opt. 7, 449 ((1998).

[103] Hamza, A. A, Sokkar, T. Z. N, Ghander, A. M, Mabrouk, M. A, & Ramadan, W. A. Pure Appl. Opt. 4, 161 ((1995).

[104] Hamza, A. A, Ghander, A. M, Sokkar, T. Z. N, Mabrouk, M. A, & Ramadan, W, A. Pure Appl. Opt. 3, 943 ((1994).

[105] Hamza, A. A, Ghander, A. M, & Mabrouk, M. A. Pure Appl. Opt. 1, 71 ((1992).

[106] Abd, R. H. El-Maksoud, M. F. Omar Appl. Opt. 50, 5957 ((2011).

[107] Hennawi, H. A, Diasty, F, Ghandoor, H, & Soliman, M. A. Opt. Quant. Electron. 43, 35 ((2012).

[108] Kahl, G. D, Mylin, D. C, & Opt, J. Soc. Am. 55, 364 ((1965).

[109] Sochacki, J, & Appl, J. Opt. 25, 3473 ((1986).

[110] Sochacki, J, Rogus, D, & Sochacka, M. Fibre Intg. Opt. 6, 279 ((1987).

[111] Hennawi, H. A, & Egypt, J. Phys. 19, 91 ((1988).

[112] Durelli, A. J, & Riley, W. F. Introduction to Photomechanics (Prentice-Hall, Englewood Cliffs, NJ, (1965).

[113] Diasty, F, & Opt, J. A: Pure Appl. Opt. 1, 197 ((1999).

[114] Diasty, F. Appl. Opt. 39, 3197 ((2000).

[115] Bertholds, A, Dandliker, R, & Lightwave, J. Technol. 6, 17-20 ((1988).

[116] Pinnow, D. A. Electrooptic materials," in Handbook of Lasers, R. J. Presley, ed. (CRC, Cleveland, Ohio, (1971).

[117] Diasty, F, & Appl, J. Phys. 87, 3254 ((2000).

[118] Diasty, F, & Opt, J. Soc. Am. A 18, 1171 ((2001).

[119] Diasty, F, & Egypt, J. Phys. 33, 359 ((2001).

[120] Diasty, F, & Opt, J. A: Pure Appl. Opt. 4, 575 ((2002).

[121] Diasty, F. Opt. Commun. 212, 267 ((2002).

[122] Diasty, F. Appl. Opt. 42, 5263 ((2003).

[123] Diasty, F. Meas. Sci. Technol. 14, 1734 ((2003).

[124] Diasty, F. Opt. Commun. 225, 61 ((2003).

[125] Diasty, F, & Opt, J. Soc. Am. A 21, 1496 ((2004).

[126] Diasty, F. F. Abdel Wahab, Opt. Eng. 45, 035003/1-7 ((2006).

[127] Diasty, F, Hennawy, H, & Soliman, M. A. Opt. Commun. 267, 394 ((2006).

[128] Diasty, F, & Amichi, A. Opt. Commun. 281, 4329 ((2008).

[129] Diasty, F, & Hennawi, H. A. Appl. Opt. 48, 3818 ((2009).

[130] Diasty, F. Opt. Eng. 51, 015007 ((2012).

[131] Abd, R. H. El-Maksoud, M. F. Omar, Appl. Opt. 50, 5957 ((2011).

[132] Malacara, D. Optical Shop Testing," Wiley: New work ((1992).

[133] Medhat, M, Zaiat, S. Y, Omer, M, & Mod, J. Opt. 43, 2205 ((1996).

[134] Medhat, M, Zaiat, S. Y, Omer, M, Barakat, N, & Mod, J. Opt. 44, 461 ((1996).

[135] Medhat, M, Zaiat, S. Y, Radi, A, Omer, M, & Opt, J. A: Pure Appl. Opt. 4, 174 ((2002).

[136] Medhat, M, Zaiat, S. Y, Saleh, M. A, Radi, A, Omer, M, & Opt, J. A: Pure Appl. Opt. 4, 485 ((2002).

[137] Zaiat, S. Y, & Hennawi, H. A. Meas. Sci. Technol. 7, 1119 ((1996).

[138] Marcuse, D, & Presby, H. Proc. IEEE 68, 676 ((1980).

[139] Ferrari, J. A, & Garcia, P. Appl. Opt. 39, 5667 ((1996).

[140] Presby, H. M. Appl. Opt. 20, 446 ((1981).

[141] Betts, R. A, Lui, F, & Whitbread, T. W. Appl. Opt. 30, 4384 ((1991).

[142] Chitti, Y. Graph. Model Image Proc. 59, 139 ((1997).

[143] Gureyev, T. E, Nugent, K. A, & Opt, J. Soc. Am. A 13, 1670 ((1996).

[144] Beniere, A, Goudail, F, Dolfi, D, Alouini, M, & Opt, J. Soc. Am. A 26, 1678 ((2009).

[145] Ma, J, Wang, Z, & Vo, M. Opt. Commun. 285, 3917 ((2012).

[146] Cai, Z, Liu, Q, & Yang, X. L. Opt. Laser Technol. 35, 295 ((2003).

[147] Vikram, Z. . H, & Caulfield, H. J. Appl. Opt. 46, 5137 ((2007).

[148] Gurov, I. P, & Opt, J. Technol. 67, 313 ((2000).

[149] Singh, H, & Sirkis, J. S. Appl. Opt. 33, 5016 ((1994).

[150] Gurov, I, Ermolaeva, E, Zakharov, A, & Opt, J. Soc. Am. A 21, 242 ((2004).

[151] Hamza, A. A, Sokker, T. Z. N, Farahaty, K. A, & Raslan, M. I. Poly. Test. 29, 1031 ((2010).

[152] Gurov, I, & Volynsky, M. Opt. Laser Technol. 50, 514 ((2012).